APPLICATION NOTE
doi.org/10.1002/elsa.202100143

Chemistry Europe
European Chemical Societies Publishing

Received: 13 August 2021
Revised: 8 October 2021
Accepted: 14 October 2021

Tracing structural changes in energy materials: A novel multi sample capillary setup for in house powder X-ray diffraction

Pirmin Stüble[1,2] | **Joachim R. Binder**[1] | **Holger Geßwein**[1]

[1] Institute for Applied Materials - Energy Storage Systems (IAM-ESS), Karlsruhe Institute of Technology (KIT), Eggenstein-Leopoldshafen, Germany

[2] Helmholtz Institute Ulm (HIU), Ulm, Germany

Correspondence
Pirmin Stüble, Institute for Applied Materials, Karlsruhe Institute of Technology (KIT), Hermann-von-Helmholtz-Platz 1, Eggenstein-Leopoldshafen 76344, Germany.
Email: pirmin.stueble@kit.edu

Abstract

Lithium ion batteries (LIBs) are currently a major subject of applied electrochemical research as there is a fast growing demand of electrochemical energy storage, driven by the transformation of the automotive sector and the expansion of renewable energies. One of the key strategies to improve LIBs is the optimization of the cathode active materials (CAMs). Therefore, in order to find structure property relations, both crystallographic and electrochemical properties need to be investigated and well understood. However, standard laboratory powder X-ray diffraction (PXRD) possibly comes to its limit when minor structural variations such as atomic defects, cation order, or minor impurity phases are addressed. In order to focus on such minor structural changes and to find decisive differences in crystalline properties of battery materials, a multi-sample capillary setup for a multipurpose in-house PXRD setup was developed. The latter is made up from a six-circle diffractometer, a microfocus molybdenum rotating anode, and a 2D area detector. The capillary spinner itself is made from commercial components and simple custom-made adapters. A goniometer head is installed on a rotary module and sample spinning is enabled by a 12 V gear motor. Mounted on a *xyz*-stage of the diffractometer, the position of the rotating capillary exposed to the primary beam can be varied while remaining perfectly aligned in the center of the diffractometer. Hence, by packing up to 10 different powder samples separated from each other into a single glass capillary, subsequent measurements of all samples can be carried out without remounting or readjustment. Within a series of samples, the setup is extremely reliable, precise, and accurate, while errors originating from sample displacement, misalignment, or calibration are minimized.

KEYWORDS
capillary, diffraction setup, Powder X-Ray diffraction, Rietveld refinement, sample changer, serial measurement

APPLICATION NOTE
doi.org/10.1002/elsa.202100143
Chemistry Europe
European Chemical Societies Publishing

1 | INTRODUCTION

Cathode active materials (CAMs) such as lithium nickel manganese cobalt oxides (NMC), lithium iron phosphate (LFP), or lithium nickel manganese oxides (LNMO) are central constituents of current high-performance lithium ion batteries (LIBs).[1] Redox activity of their transition metal constituents allows for reversible lithium extraction and insertion from and to the crystal structures and thus allowing for their application in LIBs and for energy storage. To improve the capacities and cyclability of batteries, cathode materials are one major focus of the current research and a profound understanding of their crystallographic properties is essential for further research progress.[2]

Powder X-ray diffraction (PXRD) is a powerful tool to observe, characterize, and understand these properties and consequently powder diffractometers are part of the basic equipment in battery research laboratories. Simple diffraction experiments are carried out in less than an hour[3] and quickly provide information about composition and impurity phases when the measured diffraction patterns are compared with databases.[4] To explore samples in detail, the Rietveld method[5,6] is applied. Within this method, crystal structures are refined against the experimental powder patterns and additional properties such as strain or size effects can be investigated.

However, the method requires good data and proper calibration of the diffraction setups. When it comes to rather small structural deviations, like, for example, lattice parameter variations of 0.5 pm and below, it is difficult to reliably compare results, especially when the data originates from different research groups. The reason is that diffractometers with varying geometries, angular resolutions, and X-ray sources are used and maintenance and calibration may differ.[6] Even data originating from a single diffractometer can be error prone when measurements are performed months apart or when readjustments or reconfigurations have been made in the meantime. Furthermore, sample preparation techniques, specimen alignment, data processing and refinement vary and may cause additional errors.

To overcome those issues an in house multi sample capillary PXRD setup was developed. In contrast to basic laboratory diffractometers,[3,7] a micro focus rotating anode with a small X-ray beam size is used as the X-ray source, which allows for the very compact arrangement and serial measurement of up to 10 samples in a single capillary, while avoiding the aforementioned sources of errors. Thus, high quality data can be obtained and minor structural changes in sets of samples can be investigated with very high precision, accuracy, and reliability. This allows to properly investigate correlations, for example to electrochemical properties and therefore decisive contributions to current battery research can be made.

2 | INSTRUMENTATION

2.1 | General diffraction setup

The powder diffraction setup is depicted in Figure 1. It is based on a six-circle diffractometer 5021 combined with an Eulerian cradle and a *xyz*-translation stage (Huber, Germany). A Pilatus 300K-W detector (Dectris Ltd, Switzerland) with a sensitive area of 253.7×33.5 mm^2 and a pixel size of 172×172 μm^2 is attached to the 2θ detector arm. The distance from the sample to the detector (D_0) can be varied from 25 cm to 100 cm. X-rays (Mo-$K_{\alpha 1,2}$) are generated by a molybdenum micro focus rotating anode (MM-007 HF, Rigaku, Japan) operated at 50 kV and 24 mA. For capillary measurements, apertures of the parallel collimated beam are open, a corresponding beam profile is shown in Figure 2. Evaluation of the beam intensity profiles shows that 97% and 99% of the photon flux are found within a radius of 1.0 mm and 1.2 mm, respectively. Optionally the collimating optic can be complemented with a germanium channel cut crystal to get monochromatic Mo-$K_{\alpha 1}$ radiation. To reduce air scattering, the X-rays are enclosed along the way to the sample by an aluminum tube purged with helium. The motion of the diffractometer axes are controlled with the SPEC software (Certified Scientific Software, USA) and the Pilatus detector is operated with the Dectris CAMSERVER software. Alignment of the specimens is facilitated by a video microscope camera attached to the Eulerian cradle.

2.2 | Multi-sample capillary spinner

The multi-sample capillary spinner is shown in Figure 3a. It is built on a 10 mm aluminium base plate with a commercial rotary module ERMB-20 (Festo, Germany) as a core element. A goniometer head 1005 and mounting 1413 (Huber, Germany) make up the sample carrier. These parts are connected to the rotary module via a self-built flange. A 12 VDC gear motor HG37 60:1 (Copal Electronics, Japan) enables spinning at about 0.5 Hz. It is connected via clutch EAMC-16-20-6-6 and casing EAMK-A-D32-28B (Festo, Germany) and another self-built flange. A conventional 12 V power supply with on/off switch is used to operate the motor. When mounted on the *xyz*-stage of the diffractometer, the capillary position focused by the primary beam can be varied by 42 mm in the *x*-direction. To shield the primary incident beam, a beam stop made from a simple steel strip glued on an angle bar is used. The rotation of the

doi.org/10.1002/elsa.202100143

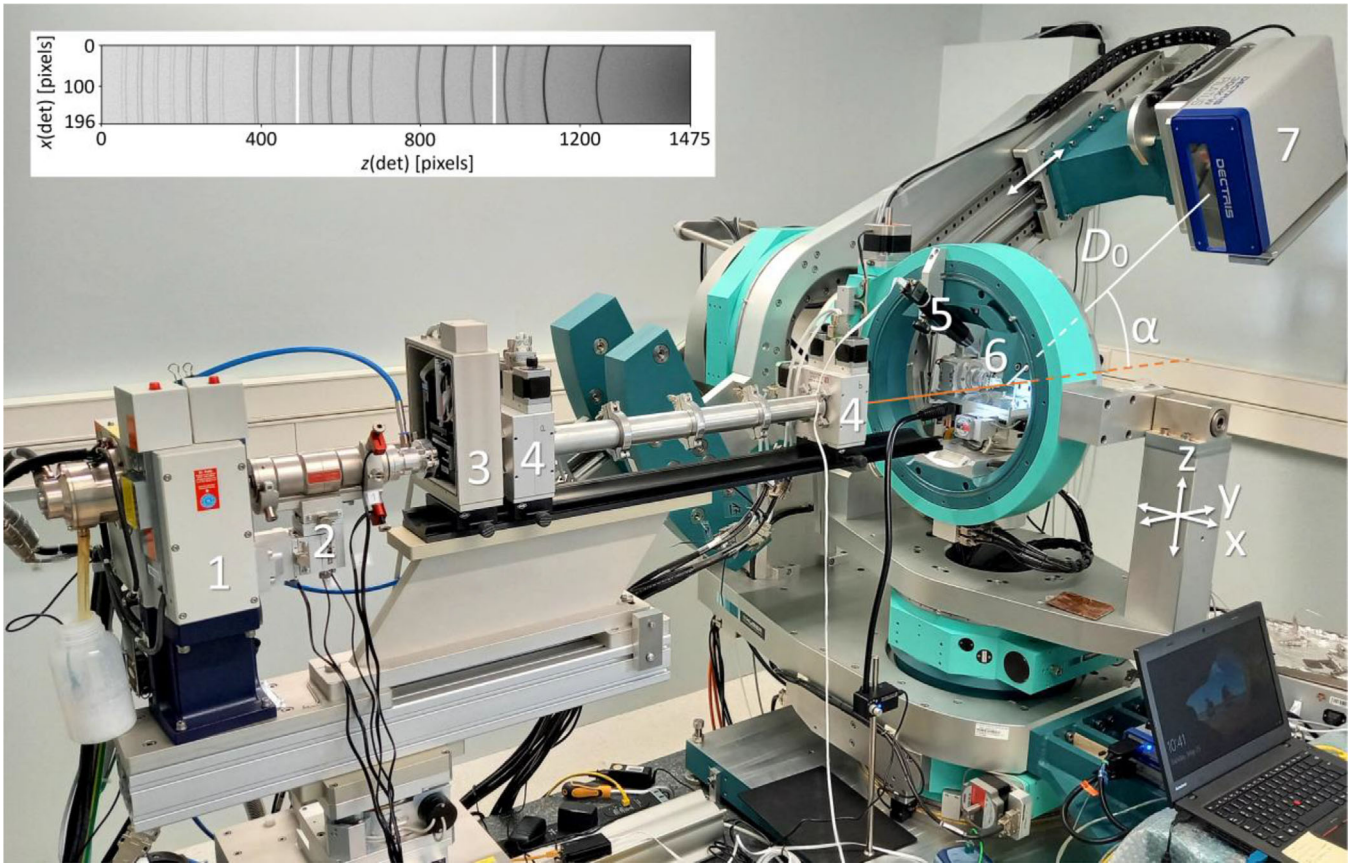

FIGURE 1 Overview of the multipurpose laboratory X-ray diffractometer. (1) X-ray source, (2) X-ray optics, (3) Ge(111) channel cut monochromator, (4) slit systems, (5) microscope camera, (6) Eulerian cradle with *xyz*-sample stage, and (7) Pilatus 300K-W area detector. The inset shows a typical 2D diffraction pattern of NIST SRM660b LaB_6 measured with the Pilatus detector. D_0 is the perpendicular distance between the sample and the detector plane and α is the tilt angle of the detector

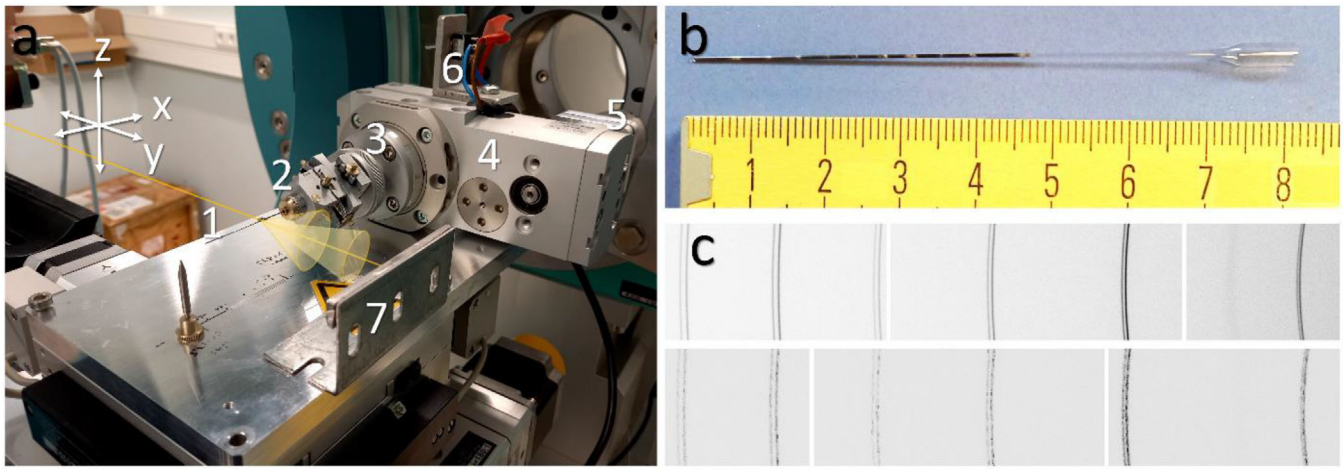

FIGURE 2 Beam profile of the attenuated direct X-ray beam on the Pilatus 2D detector (pixel size 172 × 172 μm^2), which is used for the measurement of capillary samples. The grey overlay illustrates the dimensions of a Ø = 0.5 mm capillary with a central specimen occupying 2.5 mm of space

APPLICATION NOTE
doi.org/10.1002/elsa.202100143
Chemistry Europe
European Chemical Societies Publishing

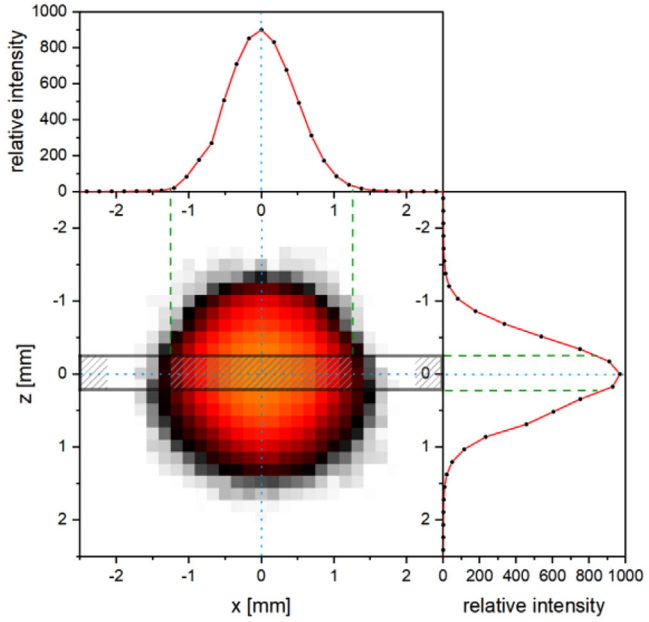

FIGURE 3 (a) Overview of the capillary spinner with a schematic drawing of the primary beam and diffracted Debye-Scherrer cones, (1) glass capillary, (2) goniometer head, (3) mounting and flange, (4) rotary module, (5) drive unit, (6) motor switch, and (7) primary beam stop. (b) Multi sample capillary filled with 10 powder samples separated by cotton wool. (c) Diffraction images of LaB_6 (NIST SRM660b) collected with (top) or without sample spinning (bottom)

capillary enables more powder crystals to meet the Bragg condition, resulting in more uniform diffraction rings, which are thus more suitable for Rietveld refinement. While negligible for nanocrystalline materials, rotation becomes crucial when materials with primary crystallite sizes of several μm are investigated (see Figure 3c and [7]).

2.3 | Sample preparation and alignment

For samples presented herein, glass capillaries made of borosilicate glass or soda lime glass (Hilgenberg, Germany) with a diameter of 0.5 mm were used. At the cost of weak reflections at $2\theta \approx 11.5°$ or 12.9° (cf. Figure 6), these capillaries provide higher mechanical stability and stiffness compared to Lindemann glass, which is often used in XRD applications. In general, the capillary diameter can be adapted to the samples examined and the use of other capillary materials, such as Kapton or Lindemann glass and quartz glass, is of course conceivable, as long as no strong bending of the horizontally aligned capillary occurs. For a detailed discussion of capillary diameters and materials and some basic considerations on capillary preparation, the reader is referred to Whitefield.[7] Given the dimensions of the beam and the possible *x*-translation of 42 mm of the sample stage (see Figures 2 and 3), capillaries can be filled in principle with 14 different samples, when each specimen occupies a length of 2 mm and the individual specimens are separated by 1 mm from each other. For practical applications however, 10 samples appear to be the upper limit for reliable handling (Figure 3b). Capillaries are filled alternating with powder samples and cotton wool. Glass fibers allow to push the wool into the capillaries and small saw blades are used to generate vibration, which facilitates the filling and compacting of the powders. Depending on the density and compaction, sample quantities of about 1-3 μg are required, which can be reduced by using thinner capillaries. After filling, the capillaries are sealed off with a lighter and fixed in wax filled brass pins suitable for the goniometer head. After mounting, the capillaries are aligned parallel to the *x*-axis and are centered. Bending and wobbling of the rotating capillary can be reduced reliably to less than 50 μm for all capillary positions. Given the large sample-to-detector distances, the resulting displacement errors do not affect the patterns significantly.[9] After this optical alignment procedure of the capillary, the *x*-positions of the sample stage, that is, the positions where the X-ray beam hits the different samples, need to be determined with the aid of the video microscope. A SPEC script, which controls the diffractometer movements, is then used to measure automatically all the powder samples contained in the capillary.

2.4 | Data acquisition and reduction

After starting the measuring script, a consecutive measurement of all samples in the capillary is performed automatically. The first sample is positioned in the center of the primary beam and the corresponding diffraction images are recorded. By translating the *x*-axis of the *xyz*-stage, the next sample is centered in the primary beam and a new measurement cycle is started. This procedure is repeated until diffraction images for all samples in the capillary are recorded. In practice, it has proven advantageous to carry out several runs with shorter exposure times for each detector position and to finally sum the different images.

To lower background noise resulting from cosmic rays, two consecutive images are summed up by applying a spike filter.[10] 1D-diffraction patterns for further data analysis are obtained by azimuthal integration using the Python based pyFAI library.[11] The integration process requires prior calibration of the diffraction setup. Therefore, a measurement of a standard reference material such as LaB_6 (NIST SRM 660b) has to be carried out and evaluated by the pyFAI-calib2 software.[11] The data reduction process is illustrated in Figure 4. The calibration process also yields the instrumental resolution function (IRF). The IRF allows

APPLICATION NOTE
doi.org/10.1002/elsa.202100143
Chemistry Europe
European Chemical Societies Publishing

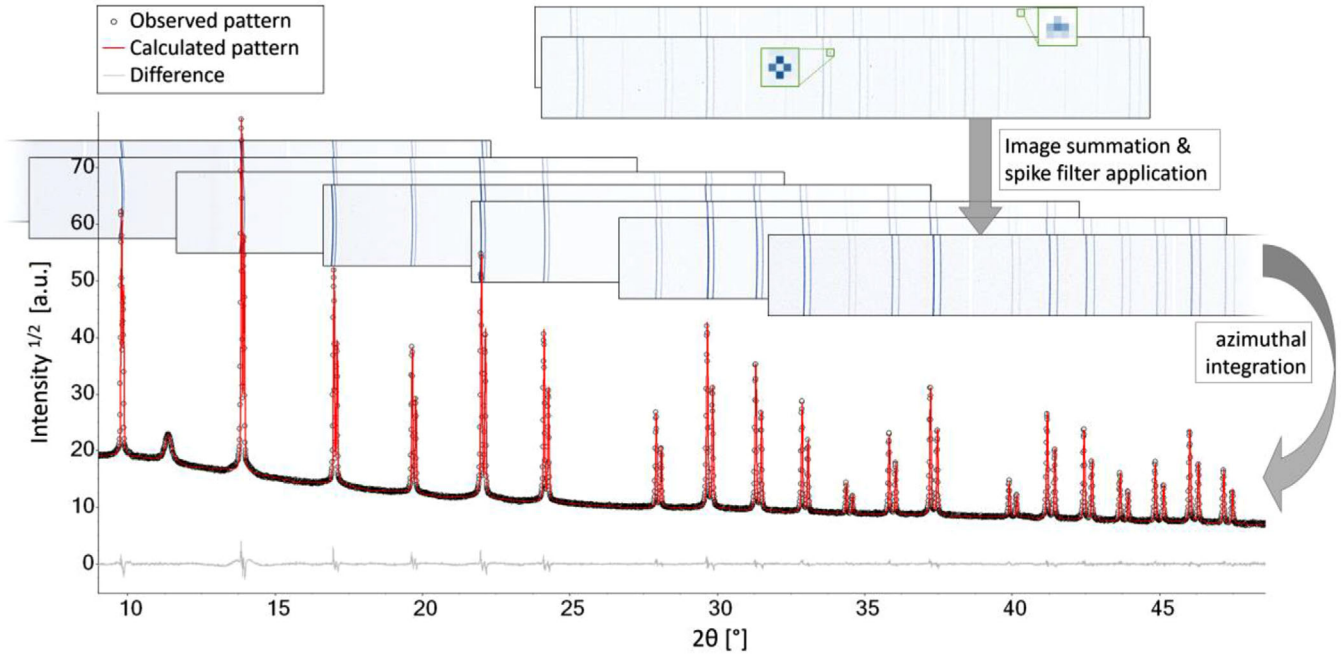

FIGURE 4 Data acquisition and processing for the capillary setup illustrated for LaB_6 (NIST SRM 660b). Detector distance 0.7 m, detector tilt angle α: 12 to 42°, 5° steps, 0.5 mm capillary diameter, Mo-$K_{\alpha 1,2}$-radiation. Several short exposures (with cosmic spikes, exemplarily highlighted in green boxes) are summed. The resulting powder diffraction pattern (black circles) is obtained by azimuthal integration of the summed spike-free images. The red line shows the refined diffraction pattern. The reflection at ~12° 2θ originates from the glass capillary

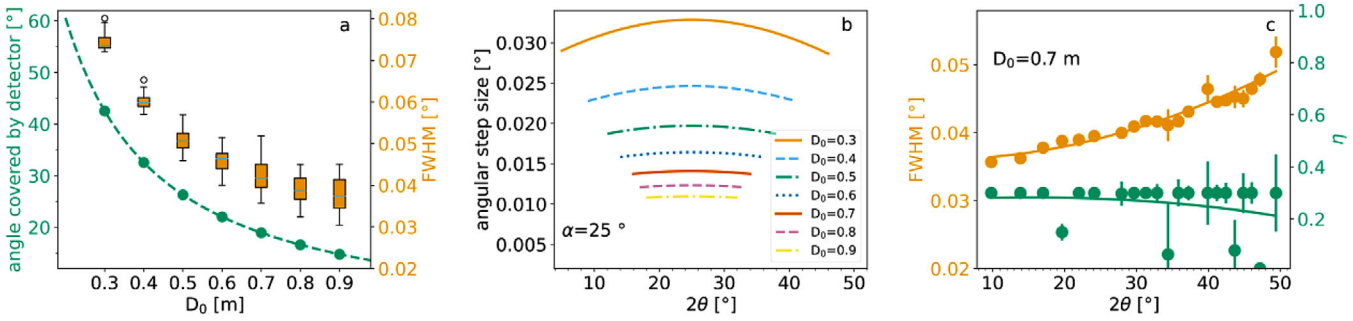

FIGURE 5 (a) 2θ angles covered by the Pilatus 300K-W detector as a function of the perpendicular sample-to-detector distance D_0 and measured range of instrumental FWHMs for SRM660b LaB_6 at each distance. (b) Calculated angular step sizes for a fixed detector tilt angle of $\alpha = 25°$. (c) FWHM curve for LaB_6 at a detector distance $D_0 = 0.7$ m together with the nearly constant trend of the Lorentzian fraction η. Solid lines are fits using the Cagliotti equation $\mathrm{FWHM}(\theta) = \sqrt{u\tan^2(\theta) + v\tan(\theta) + w}$ and $\eta(\theta) = a + b\theta + c\theta^2$ [13]

for the analysis of microstructural effects such as lattice defects, microstrain, or domain size effects. For Rietveld refinements, the TOPAS V6 Software (Bruker) is used.

2.5 | Angular step size and instrumental resolution function

The angular step size of the diffraction patterns obtained from the integrated Pilatus detector images depends on the sample-to-detector distance and the pixel size of the detector. For flat detectors, this step size can be estimated as: $\Delta 2\theta(2\theta) = (180/\pi)\{[\mathrm{pix} \times \cos^2(2\theta - \alpha)]/D_0\}$, where pix is the pixel size of the detector, α is the tilt angle of the detector, and D_0 is the perpendicular distance between the sample and the detector plane.[12] The 2θ range that can be covered with a single exposure of the Pilatus detector depends on the sample-to-detector distance and typically decreases when the distance is increased. The angular coverage of the Pilatus detector as a function D_0 is shown in Figure 5a. It decreases from 42.5° at $D_0 = 0.3$ m to 14.8° at $D_0 = 0.9$ m. The angular step size, which contributes

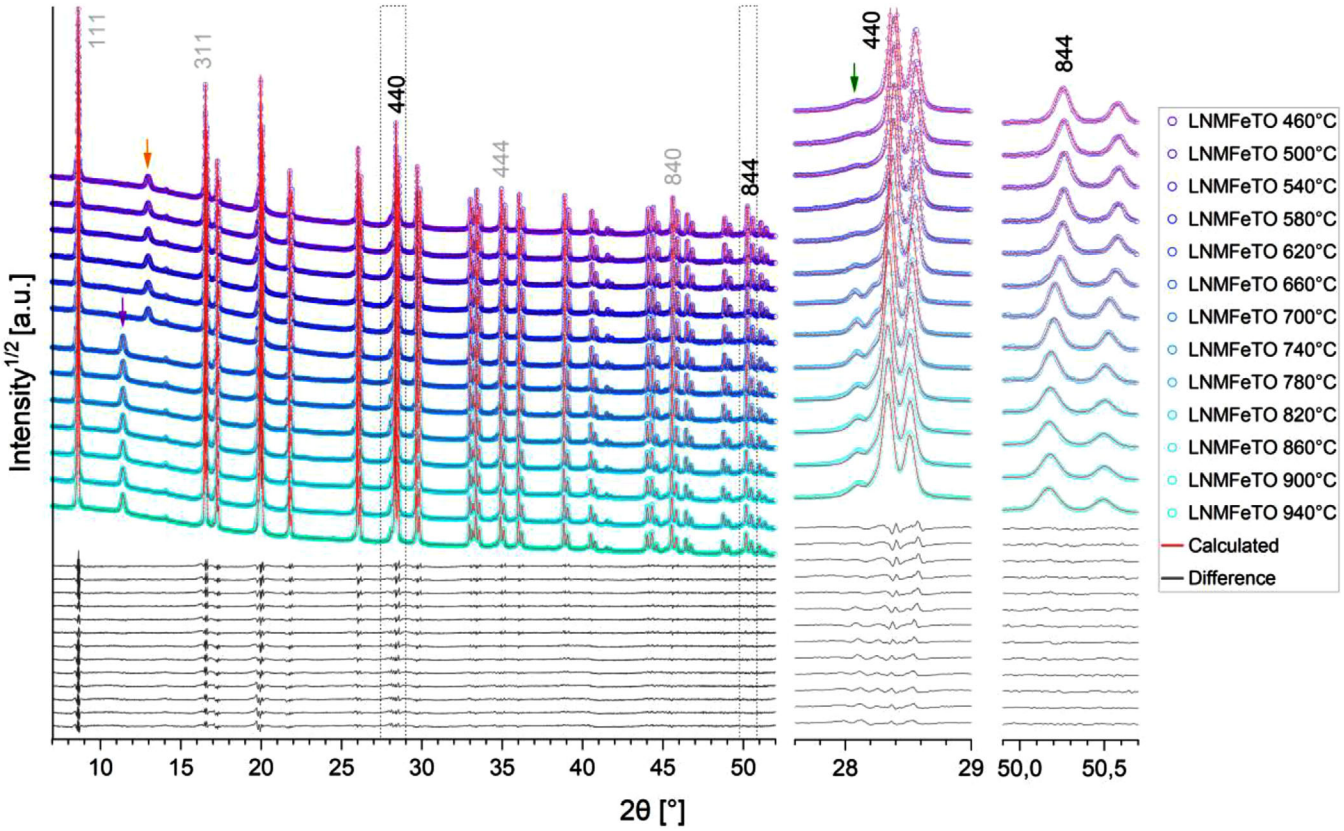

FIGURE 6 Diffraction patterns and corresponding Rietveld refinement results of a series of Fe-Ti doped LNMO spinel samples obtained from the measurements of two multi sample capillaries with enlarged 2θ ranges around 28.5° and 50°. Small changes of the weight fraction of the secondary phase (marked with a green arrow) and the lattice parameter of LNMO (peak shift of the 844 reflection) can be observed. Double reflections result from $K_{\alpha 1}$-$K_{\alpha 2}$-splitting. Black and gray numbers represent selected reflection indices of the spinel phase. Purple and orange arrows indicate the contributions of the borosilicate and soda lime glass capillaries

to the instrumental profile broadening, is in the order of 0.01° for high distances of 0.9 m and increases to values of about 0.03° when the detector is positioned at 0.3 m to the sample (see Figure 5b). For larger sample-to-detector distances, several diffraction images collected at different tilt angles of the detector need to be merged and integrated to a 1D diffraction pattern that covers the required 2θ range. The experimental line profile measured from the NIST SRM660b LaB_6 standard at a distance of 0.7 m is shown in Figure 4. The 1D diffraction pattern is the result of a merger of seven images collected at tilt angles ranging from 12° to 42° in 5° steps. The observed line profiles can be described with symmetrical pseudo-Voigt functions. The instrumental resolution in terms of the FWHMs (full width at half maximum) of the SRM660b LaB_6 reflections for the capillary (Debye-Scherrer) geometry as a function of the sample-to-detector distance is summarized in Figure 5a. It is evident that the instrumental profile widths decrease from ~0.075° to ~0.035° when the detector distance is increased from 0.3 to 0.9 m. Details of the dependence of the FWHMs on the scattering angle as well as the Lorentzian fraction (η) of the pseudo-Voigt function[13] used in the profile fitting are seen in Figure 5c. Here, a detector distance D_0 of 0.7 m is selected, as this is the most common distance for the multi-sample capillary setup.

3 | APPLICATION RESULTS

The capillary setup was used for a new study of the influence of the calcining temperature on the crystallographic and electrochemical properties of an iron titanium doped LNMO spinel ($LiNi_{0.5}Mn_{1.37}Fe_{0.1}Ti_{0.03}O_{3.95-\delta}$) cathode material that had been subject of earlier research.[14] Therefore, a series of 13 samples were calcined at temperatures between 460°C and 940°C in steps of 40°C. Two capillaries were each filled with small quantities of six and seven samples and were then investigated with the described PXRD setup. The measured diffraction patterns and Rietveld refinement results are depicted in Figure 6.

The refined lattice parameter a of the spinel phase and the phase fraction of the secondary phase ($Li_{1-x}Ni_xO$,

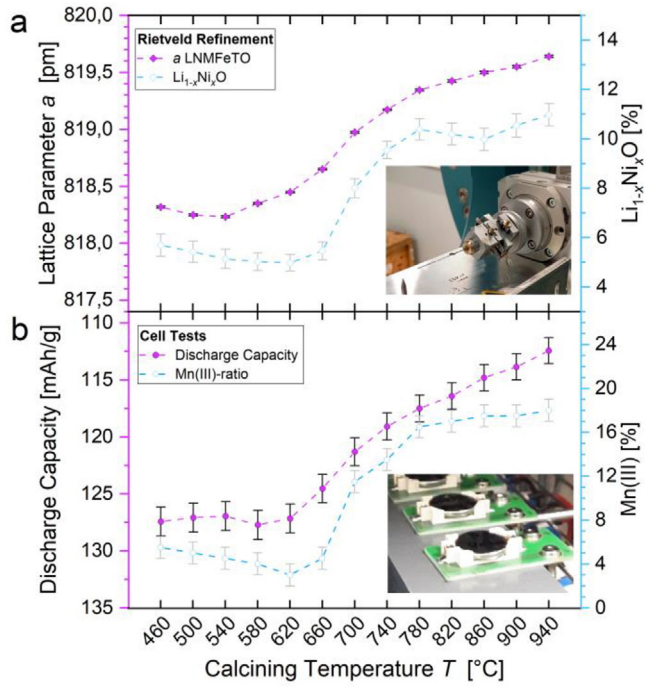

FIGURE 7 Structure property correlation of a Fe-Ti doped LNMO battery material. (a) Lattice parameter a and secondary phase fraction obtained from X-ray powder diffraction (multi capillary setup). (b) Discharge capacity and Mn(III) content derived from cell testing

$x \approx 0.3$) are depicted in Figure 7a. Electrodes were prepared from the calcined materials and the electrochemical properties were investigated by galvanostatic cycling of coin cell batteries with lithium foil as anodes. The Mn(III) content was derived from the voltage profiles of the second cycle (0.1 C) and the discharge capacities at 1C were determined (referring to a theoretical capacity of 147 mAh/g). The results are given in Figure 7b and show correlations between the lattice parameter and the discharge capacity and between the phase fraction of the secondary phase and the Mn(III) content derived from the voltage profiles. Roughly simplified, it can be concluded that higher calcining temperatures favor the formation of Mn(III) rich LNMO phase, and increased ratios of the $Li_{1-x}Ni_xO$ secondary phase. In turn, the discharge capacity of the LNMO material decreases. The combination of crystallographic and electrochemical characterization methods thus yields detailed insights into the properties of the cathode active material and can therefore help to improve it for possible future applications.

4 | CONCLUSION

We have developed and installed a multi sample capillary spinner for a multipurpose laboratory powder X-ray diffractometer. The setup allows automated serial measurements of up to 10 powder samples prepared in a single glass capillary while systematic sources of error, such as misalignment or sample displacement errors are minimized. For typical measurements (Ø = 0.5 mm capillary, Mo-$K_{\alpha 1,2}$ radiation, $D_0 = 0.7$ m) sample quantities of only 1–3 μg are required and diffraction patterns with a high angular resolution of about 0.04° 2θ FWHM can be obtained. While the effort for filling a multi sample capillary is similar to preparing a corresponding number of individual capillaries, the work involved on the diffractometer is drastically reduced compared to individual measurements. Within a series of samples, minute differences in crystalline materials are detectable. The setup thus expands the scope of laboratory X-ray diffraction techniques and is an excellent tool for investigating structure property relations. The setup has been in operation since 2019 and has proven to be very reliable and accurate. Currently, it is mainly used to improve the understanding of calcining processes and doping effects of LNMO battery materials, however, a variety of applications, like the investigation of air sensitive samples are conceivable.

ACKNOWLEDGMENTS

The authors would like to thank Bertram Kuntz and the staff at KIT-TEC for their help with the technical implementation. The work contributes to the research performed at CELEST (Center for Electrochemical Energy Storage Ulm-Karlsruhe).

CONFLICT OF INTEREST

The authors declare no conflict of interest.

DATA AVAILABILITY STATEMENT

The data that support the findings of this study are available from the corresponding author upon reasonable request.

REFERENCES

1. B. Xu, D. Qian, Z. Wang, Y. S. Meng, *Mater. Sci. Engi. R Rep.* **2012**, *73*, 51.
2. J. Meng, H. Guo, C. Niu, Y. Zhao, L. Xu, Q. Li, L. Mai, *Joule* **2017**, *1*, 522.
3. A. Kern, *International Tables for Crystallography Volume H: Powder Diffraction* (Eds: C. J. Gilmore, J. A. Kaduk, H. Schenk), International Union of Crystallography, **2019**, pp. 26–50.
4. J. A. Kaduk, in *International Tables for Crystallography Volume H: Powder Diffraction* (Eds: C. J. Gilmore, J. A. Kaduk, H. Schenk), International Union of Crystallography, **2019**, pp. 304.
5. H. M. Rietveld, *Acta Crystallogr.* **1967**, *22*, 151.
6. L. B. McCusker, R. B. Dreele, D. E. Cox, D. Louër, P. Scardi, *J. Appl. Crystallogr.* **1999**, *32*, 36.

7. P. S. Whitfield, A. Huq and J. A. Kaduk, in *International Tables for Crystallography Volume H: Powder Diffraction* (Eds: C. J. Gilmore, J. A. Kaduk, H. Schenk), International Union of Crystallography, **2019**, pp. 200–222.
8. P. Scardi, *Powder Diffraction* (Eds: R. E. Dinnebier, S. J. L. Billinge), Royal Society of Chemistry, Cambridge, **2008**, pp. 376–413.
9. N. V. Y. Scarlett, M. R. Rowles, K. S. Wallwork, I. C. Madsen, *J. Appl. Crystallogr.* **2011**, *44*, 60.
10. H. Takeuchi, S. Hashimoto, I. Harada, *Appl. Spectrosc.* **1993**, *47*(1), 129.
11. J. Kieffer, J. P. Wright, *Powder Diffr.* **2013**, *28*, S339.
12. P. Norby, *J. Appl. Crystallogr.* **1997**, *30*, 21.
13. P. Scardi, *Cryst. Growth Des.* **2020**, *20*, 6903.
14. A. Höweling, A. Stoll, D. O. Schmidt, H. Geßwein, U. Simon, J. R. Binder, *J. Electrochem. Soc.* **2017**, *164*, A6349.

How to cite this article: P. Stüble, J. R. Binder, H. Geßwein, Tracing structural changes in energy materials: A novel multi sample capillary setup for in house powder X-ray diffraction, *Electrochem. Sci. Adv.* **2021**, e2100143.
https://doi.org/10.1002/elsa.202100143